

Multi-modal therapeutic action of gallium-containing bioactive glass against osteosarcoma and bacterial pathogens

Lucas Pereira Lopes de Souza^{a,b,*}, Joao Henrique Lopes^c, Luis Felipe Moreira Oliveira^c, Farah Naz Safdar Raja^{b,d}, Archana Singh^e, Shirin Hanaei^b, Darrell Green^f, Adrian Gardner^{a,g}, Jonathan Stevenson^a, Richard Alan Martin^b

^a Department of Research, Audit, & Development, The Royal Orthopaedic Hospital NHS Foundation Trust, B31 2AP Birmingham, United Kingdom

^b School of Engineering & Physical Sciences, Aston University, B4 7ET Birmingham, United Kingdom

^c Biomaterials and Biointerfaces Laboratory (BBLab), Department of Chemistry, Division of Fundamental Sciences (IEF), Aeronautics Institute of Technology, São José dos Campos, São Paulo 12228-900, Brazil

^d College of Medicine and Dentistry, Outreach Centre of Ulster University, Birmingham, United Kingdom

^e Amity Institute of Biotechnology, Amity Institute of Integrative Sciences and Health, Amity University Haryana, Gurugram, India

^f Norwich Medical School, University of East Anglia, Norwich Research Park, NR4 7UQ Norwich, United Kingdom

^g Aston Medical School, Aston University, B4 7ET Birmingham, United Kingdom

ARTICLE INFO

Keywords:

Bone tumour
Bioactive glass
Gallium
Cytotoxicity
Apoptosis
RNA-sequencing

ABSTRACT

Despite multimodal therapy, bone tumours can lead to high morbidity and poor survival, with recurrent limited success from trials investigating targeted or immunotherapies. Surgery remains essential and is often the only option available for refractory disease, skeletal metastases, and some benign bone lesions. However, primary bone tumours, such as osteosarcoma, often recur locally when complete resection is hindered by limited safety margins or proximity to vital structures. A multifunctional biomaterial capable of eradicating residual tumour cells while promoting bone regeneration could significantly improve outcomes of surgical procedures in these clinical settings. Here, we report the anticancer and antibacterial properties of gallium-containing bioactive glasses (Ga-BGs). We show that osteosarcoma cell lines are especially sensitive to gallium and that Ga-BGs can release therapeutic levels of gallium ions that selectively kill osteosarcoma cells. Our mechanistic investigation reveals that gallium promotes a multi-pronged molecular attack on key hallmarks of cancer cells, primarily through disrupting iron metabolism leading to increased oxidative stress, induction of cell death pathways, and suppression of oncogenic and metastatic signalling. Moreover, gallium nitrate and Ga-BGs are shown to present inhibitory effects upon gram-negative bacteria *P. aeruginosa*. Taken together, our results indicate that Ga-BGs constitute a model biomaterial for the development of multi-functional scaffolds for the treatment of osteosarcoma.

1. Introduction

Standard treatment for malignant primary bone tumours typically involves *en-bloc* surgical excision with or without reconstruction, and combinations of chemo-radiotherapy depending upon histological type [1,2]. However, therapeutic progress has stagnated over the past four decades, with five-year overall survival rates remaining around 50 % [3]. Effective disease management remains challenged by high rates of implant failure, infection, and local recurrence, particularly in cases where *en bloc* resection or radiotherapy is limited by inadequate safety margins or proximity to critical structures [1,4,5]. Intralesional or compromised margins are frequently encountered and may result in substan-

tial bone loss with and increased risk of local recurrence. There is consequently a pressing need for biomaterials capable of eradicating residual tumour cells while supporting osteogenesis, especially at sites unsuitable for curative surgery or radiotherapy, such as close to the spinal cord or other vital viscera [6,7]. Such materials could be integrated with minimally invasive ablative modalities, including cryoablation, to improve local control and functional outcomes [6].

Bioactive glasses represent the gold-standard synthetic grafting material for bone formation and have been deployed in more than one million patients worldwide for bone repair [8]. The rapid bone formation elicited by this material is related to two mechanisms: (a) spontaneous formation of crystalline hydroxyl carbonate apatite (HCA) on the

Peer review under the responsibility of editorial board of Engineered Regeneration.

* Corresponding author at: Department of Research, Audit, & Development, The Royal Orthopaedic Hospital NHS Foundation Trust, B31 2AP Birmingham, United Kingdom

E-mail address: lucas.souza@nhs.net (L.P.L. de Souza).

<https://doi.org/10.1016/j.engreg.2026.05.001>

Received 7 January 2026; Received in revised form 29 April 2026; Accepted 1 May 2026

Available online 2 May 2026

2666-1381/© 2026 The Authors. Publishing Services by Elsevier B.V. on behalf of KeAi Communications Co. Ltd. This is an open access article under the CC BY-NC-ND license (<http://creativecommons.org/licenses/by-nc-nd/4.0/>)

material's surface upon reaction with physiological fluid such as saliva or blood, etc.; and (b) the stimulation of cellular activity by its ions, released in the aqueous medium, promoting enhanced bone formation [8]. One of the main advantages of bioactive glasses is the amorphous nature of their matrix that allows for easier incorporation and controlled release of different therapeutic metallic ions. The fast expansion in the clinical use of bioactive glasses has prompted researchers to start looking for possible ions with anticancer properties for cancer applications. Concomitantly, in a series of investigations with different metallic ions, the ion gallium stood out as a promising candidate for cancer therapy [9]. Gallium was initially utilized solely for imaging bone tumours. However, in 1969, after discovering that ^{67}Ga could accumulate in soft tissue tumours, it became valuable in treating Hodgkin's lymphoma. By the mid-1970s, gallium nitrate had reached clinical trials, making gallium the second metal, after platinum, to exhibit therapeutic activity in patients with cancer [10–13]. Combining gallium with biomaterials enhances targeted delivery to the affected area while reducing harmful systemic side effects. Our early work demonstrated the bone forming and selective anticancer potential of gallium-doped bioactive glasses upon a single cell line of osteosarcoma (Saos2) as well as its biocompatibility and osteointegration potential in treating critical-sized calvarial defects in rats [14–16].

The present article describes a comprehensive investigation which, for the first time, determined the existence of a therapeutic window for gallium in multiple primary bone cancer cells and the potential of gallium-containing bioactive glasses (Ga-BGs) to release gallium within this pre-determined dose range and selectively kill those cell lines. Furthermore, we report results from a thorough enquiry on the molecular mechanism of action of gallium, unravelling the intracellular pathways involved in the observed ion-dependent selective cell death. This article also reports results from an investigation of the antibacterial properties of gallium and Ga-BGs. To conclude, a mechanistic model is proposed to describe how Ga-BGs can serve as ideal drug delivery systems for gallium ions and act as a multi-functional agent to simultaneously regenerate bone, kill bone cancer cells, and prevent bacterial colonisation.

2. Materials and methods

2.1. Preparation of gallium-containing bioactive glasses

The gallium-doped bioactive glasses employed in this investigation were manufactured by modifying the original Bioglass 45S5 composition [17]. The alteration specifically involved incorporating 1–5 mol% of Ga_2O_3 at the expense of SiO_2 , whilst ensuring the appropriate rate of dissolution. A comprehensive description of the structural formulation of gallium-doped glasses can be found in the supporting information (SI.1). The standard melt quench route was utilized for sample preparation. In summary, precise quantities of SiO_2 (Alfa Aesar, 99.5 %), $\text{NH}_4\text{H}_2\text{PO}_4$ (Sigma-Aldrich, 99.5 %), CaCO_3 (Alfa Aesar, 99.95–100.05 %), Na_2CO_3 (Sigma-Aldrich, 99.5 %), and Ga_2O_3 (ACROS Organics™, 99.99+ %) were thoroughly blended in a 90 % Pt–10 % Rh crucible at room temperature. The mixture was then transferred to a high-temperature furnace, heated to 1450 °C at a rate of 10 °C/min. Subsequently, the molten glass was held at 1450 °C for 90 min and rapidly cooled by pouring into ultrapure water at 25 °C. Glass frits were thoroughly dried before using a vertical planetary ball mill (XQM systems, Changsha, China) at a rotation frequency of 350 rpm/min to prepare powdered glass samples. The fraction of glass with a diameter between 40 and 63 μm was selected through sieving for further experimental procedures.

2.2. Characterization of gallium-containing bioactive glasses

2.2.1. Solid-state MAS NMR and Raman spectroscopy

The chemical environments of 45S5 and the structural modifications induced by gallium incorporation along the gallium-containing glass se-

ries were analysed by solid-state MAS NMR spectroscopy, probing the ^{29}Si nucleus. MAS NMR experiments were conducted using a Fourier Transform NMR spectrometer (Bruker AVANCE II+ 400, 9.04 T; Bruker, Rheinstetten/Karlsruhe, Germany) operating at resonance frequencies of 79.49 MHz. Standard Bruker double-resonance magic-angle spinning (MAS) probes were employed. Glass powder samples were packed into 4-mm cylindrical zirconia rotors and spun at 10 kHz at the magic angle to minimize anisotropy effects. All NMR spectra were recorded at ambient probe temperatures using a high-power decoupling (HPDEC) pulse sequence for ^1H The ^{29}Si MAS NMR spectra were acquired using 1.5 μs pulses, 82 ms acquisition times, and 40 s recycle delays, with a spectral width of 25 kHz and a total of 4096 scans collected. Tetramethylsilane (TMS) was used as an external reference. The recorded spectra were processed using TopSpin 2.1.6 software by applying Fourier transformations and exponential filters of 100 Hz for ^{29}Si . The phase was manually corrected, and the baseline was adjusted using a fifth-order polynomial function. To ensure the reliability of the data, repeated measurements were performed on samples from different batches. The short-range order analysis was obtained using a triple spectrometer Raman system (T-64,000, HORIBA Jobin Yvon S.A.S., Longjumeau, France) equipped with a Charge-Coupled Device (CCD) detection system. The measurements employed a confocal microscope (BX41, Olympus Optical Co. Ltd., Tokyo, Japan) operating in a backscattering geometry, utilizing a 100x objective for efficient Raman signal collection. The spectral analysis was performed with a spectrometer offering a resolution of approximately 2 cm^{-1} . Raman spectra were recorded within the range of 200 to 1300 cm^{-1} using a 532 nm excitation wavelength. The illumination power was set to 20 mW to ensure optimal signal intensity. For each sample, 15 measurements were performed with an integration time of 30 s.

2.2.2. Inductively coupled plasma - optical emission spectroscopy (ICP-OES)

The dissolution behaviour of bioactive glasses is strongly influenced by the network connectivity (NC), which reflects the degree of polymerization of the silicate network and controls the release of ionic species from the glass matrix. In the present work, all glass compositions were designed to maintain a similar NC value (~ 2.1), comparable to that of the reference 45S5 bioactive glass, to ensure a consistent dissolution behaviour across the compositional series. ICP-OES was used to measure the concentrations of ionic dissolution products released from a serial dilution of $\text{Ga}(\text{NO}_3)_3$ and from gallium-containing bioactive glasses (Ga-BGs). For that, a serial dilution with halving intervals of $\text{Ga}(\text{NO}_3)_3$ in distilled water was performed from 1000 $\mu\text{g}/\text{mL}$ to 7.8125 $\mu\text{g}/\text{mL}$, then filtered using 0.22 μm syringe filter. For the Ga-BGs, stock solutions were prepared at 10 mg/mL in distilled water and incubated in a shaker incubator at 36.5 °C with 200 rpm for 24 h. Following incubation, the solutions were filtered using a 0.22 μm syringe filter to remove glass particles. Nitric acid was added to the samples to stabilize the elemental components in solution. Analysis was performed with an ICP-OES (iCAP 7000 Plus Series). Calibration curves were generated by diluting reference standards of Ga^{3+} , Si^{4+} , Ca^{2+} , and Na^+ to concentrations of 1, 10, 20, and 100 $\text{mg}\cdot\text{kg}^{-1}$ in distilled water. Ion concentrations were determined using the linear range of the standard curves. All measurements were performed in triplicate.

2.3. Cell culture

Normal bone cells were represented by Human Osteoblasts (NHObTs, CC-2538, Lonza) and Human Foetal Osteoblasts (hFOB 1.19, CRL-3602, ATCC), whereas the cell lines HOS (ATCC CRL-1543), MNNG/HOS (ATCC CRL-1547), Saos2 (ATCC HTB-85), 143B (ATCC CRL-8303) and SJS-1 (ATCC CRL-2098) represented human osteosarcoma cells. NHObTs cells were cultured in OGM™ Osteoblast Growth Medium BulletKit™ (Lonza, Catalog #: CC-3207) whilst hFOB cells were grown in Dulbecco's Modified Eagle's Medium (DMEM) (Gibco, 41,966,029)

supplemented with 10 % foetal bovine serum (FBS) (ATCC 30–2020). HOS and MNNG/HOS cells were grown in Eagle's Minimum Essential Medium (ATCC 30–2003) supplemented with 10 % FBS (ATCC 30–2020). 143B cells were cultured in Dulbecco's Modified Eagle's Medium (DMEM) (Gibco, 41,966,029) supplemented with 10 % FBS (ATCC 30–2020). Saos2 cells were cultured in McCoy's 5A medium (ATCC 30–2007) with 15 % FBS (ATCC 30–2020). SJS-1 cells were cultured in RPMI medium (ATCC 30–2001) supplemented with 10 % FBS (ATCC 30–2020). All cell lines were maintained in a controlled environment at 36.5 °C with 5 % CO₂ apart from hFOB cells which were grown at 34.5 °C. For all cell lines, cell culture medium was fully replenished every other day and regularly checked to be *Mycoplasma* free. All cells used in this study were obtained from commercial suppliers and the Royal Orthopaedic Hospital R&D Governance office granted exemption from formal ethical approval for their use. All experimental procedures were conducted in strict accordance with UK legal requirements and institutional guidelines governing the use of commercially sourced human cells.

2.4. Treatment regimes

To test the cytotoxicity of gallium-containing bioactive glasses (Ga-BGs), culture media were conditioned with Ga-BG powders at concentrations of 10 mg/mL. To achieve this, the appropriate amount of powder was added to the respective basal medium and mixed at 220 RPM at 36.5 °C for 24 h. Following incubation, the appropriate amount of FBS was added to the medium to make it complete. The mixture was then filtered using an ultrafine filter with a 0.22 µm pore size (Corning, # 431,229) and placed in a 5 % CO₂ incubator overnight at 36.5 °C to acclimatize and buffer the pH before being utilized to treat cells in subsequent experiments. Similarly, culture media were conditioned with gallium nitrate. For that, a serial dilution with halving intervals of Ga(NO₃)₃ in complete medium was performed from 1000 µg/mL to 7.8125 µg/mL, then filtered using an ultrafine filter (Corning, #431,229) with a 0.22 µm pore size and incubated at 36.5 °C, 5 % CO₂ overnight.

2.5. MTT assay

To quantify the viability of cells subjected to the different treatments, cells were seeded into 96-well plates (Falcon®, #353,072) at a seeding density of 10,000 cells/cm² (3200 cells/well). After overnight attachment, cells underwent treatment with gallium nitrate or glass-conditioned media for 3, 5, and 7 days. Cells treated with their appropriate growth medium served as negative controls whilst cells killed with 70 % ethanol served as positive control. Media were not replenished during treatment duration. After the appropriate treatment time, MTT assay was conducted. In short, medium was removed from each well and replaced with 100 µL of a 1:10 (1.2 mM) solution of 3-(4,5-Dimethylthiazol-2-yl)-2,5-Diphenyltetrazolium Bromide (MTT) (Invitrogen, #M6494) and phenol-free Dulbecco's Modified Eagle Medium (DMEM) (Gibco, # 21,063,029). The plates were then incubated for 4 h at 36.5 °C in a 5 % CO₂ incubator. Succinate dehydrogenase produced by viable, metabolically active cells reacted with MTT, resulting in the formation of insoluble purple formazan within cells. Dissolving the precipitated formazan involved replacing 75 µL from each well with 50 µL of dimethyl sulfoxide (DMSO) (Thermo Scientific, Catalog number: 022,914.K2) and incubating for 10 min at 36.5 °C in the 5 % CO₂ incubator. Optical density measurements at 540 nm were taken using a microplate reader (Thermo Scientific, Multiskan GO). This entire experiment was conducted in triplicate (6 wells per plate, 3 × 96-well plates). A Kolmogorov–Smirnov test was applied to assess the normality of data distribution. Subsequently, a one-way ANOVA test followed by Dunnett's test were applied to compare the experimental groups, maintaining a 95 % confidence interval for all group comparisons.

2.6. Live/Dead assay

To qualitatively assess the viability of cells subjected to the different treatments, cells were seeded at a density of 10,000 cells/cm² (3200 cells/well) into a 96-well plate (Falcon, # 353,072). After overnight attachment, cells were subjected to treatment with glass-conditioned (at 10 mg/mL) or gallium nitrate-conditioned media for 7 days. Following this treatment period, a LIVE/DEAD cell viability assay (Invitrogen, #L3224) was conducted. The assay was performed in triplicate. Briefly, a mixture of Ethidium Homodimer, Calcein AM, and Dulbecco's phosphate-buffered saline (DPBS) (Gibco, #14,190,094) was prepared and added to individual wells at a final concentration of 2.5 µM of EthD-1 and 0.5M of CA. Following a 30-minute incubation period at 36.5 °C, 5 % CO₂ and in the dark, the cells were photographed using an inverted fluorescence microscope (Thermo Scientific, # AMF5000) at 100x magnification.

2.7. Caspase 3/7 assay

The activation of Caspases 3 and 7 are central to caspase-dependent programmed cell death. As part of the caspase family of proteases, Caspases 3 and 7 become activated in response to specific signals and contributes to the execution phase of apoptosis. This experiment aimed to evaluate the potential of gallium-containing bioactive glasses to stimulate apoptosis in the different cell lines. For this, cells were seeded at a density of 10,000 cells per cm² (3200 cells/well) in a 96-well plate (Falcon, # 353,072). After overnight adherence, cells were treated with glass-conditioned (at 10 mg/mL) media for a duration of 7 days. Staurosporine (Thermo Scientific, #328,530,010) was added to control wells to induce cell death to serve as a comparator on Day 6 of the experiment, at the concentration of 1 µg/mL. On Day 7, 1:100 caspase 3/7 detection reagent (Invitrogen, #C10432) was added to each well and incubated for 30 min prior to imaging at 200 X magnification.

2.8. Determining minimal inhibitory concentration against *Pseudomonas aeruginosa*

Minimum inhibitory concentration (MIC) of 5 %Ga-BG and gallium nitrate was performed using broth microdilution assay, as indicated by the Clinical & Laboratory Standards Institute (CLSI) guidelines. Stock solutions were prepared (5 % Ga-BG at 25 mg/mL, gallium nitrate at 2000 µg/mL) and tested against *Pseudomonas aeruginosa* (PA14). *Pseudomonas aeruginosa* strain PA14 was kindly provided by Sarah Khuene, University of Birmingham. Double dilutions of each stock solution (5 % Ga-BG – 12.5–0.8 mg/mL, gallium nitrate – 1000–15.6 µg/mL), were performed in a 96 well plate, with a final volume of 100 µL per well. One hundred µL inoculum of 10⁵ CFU/mL was added in each well, and the concentration of the inoculum was confirmed by plating. 200 µL of broth served as negative control whereas broth containing bacterial inoculum was used a positive control. Triplicate samples were prepared and incubated at 36.5 °C in an aerobic environment. Growth was determined by measuring the optical density at 570 nm using BioTek ELx800 absorbance. The value of MIC was set as the lowest concentration to have no clearly visible growth or an average well optical density within the range of negative control well.

2.9. Transcriptomic analysis

hFOB and 143B cells were grown in 6-well plates until they reached 70–80 % confluency and were treated with Ga(NO₃)₃-conditioned medium at the concentration of 62 µg/mL for 36 h. Cells in complete medium only served as controls. Following 36 h of incubation, total RNA was extracted using Trizol. RNA concentration and purity were assessed spectrophotometrically using a NanoDrop OneC UV–Vis Spectrophotometer (Thermo Scientific, Wilmington, DE, USA). mRNA libraries were constructed using the NEBNext ultra II RNA library prep

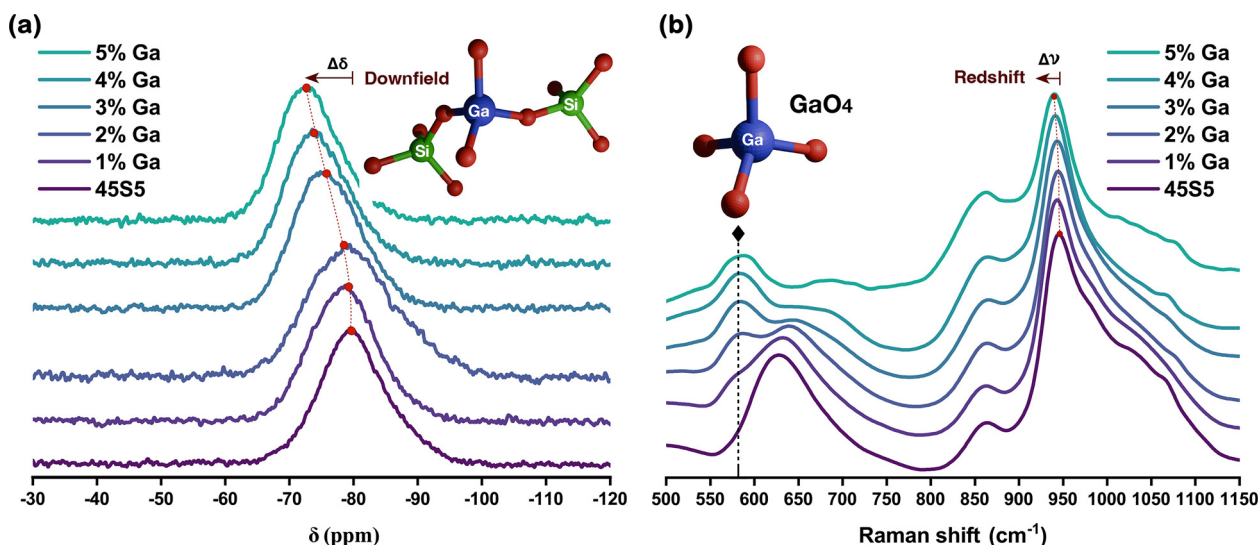


Fig. 1. ^{29}Si MAS NMR and Raman spectroscopy of Ga-BGs. (a) The progressive downfield shift observed in the ^{29}Si MAS NMR spectra with increasing Ga_2O_3 content can be rationalized in terms of electronic shielding effects. The substitution of Si-O-Si bridges by more ionic Si-O-Ga linkages reduces the electron density around the silicon nuclei, leading to decreased overall shielding (σ_{total}). This effect arises primarily from an enhancement of the paramagnetic contribution (σ_p) to the total shielding, as the incorporation of Ga^{3+} lowers the energy separation between occupied and unoccupied molecular orbitals involved in Si-O-Ga bonding. The smaller energy gap facilitates virtual electronic excitations, increasing σ_p , which in turn dominates over the relatively constant diamagnetic term (σ_d). Consequently, the reduced shielding of the ^{29}Si nuclei results in a systematic downfield displacement (less negative δ values) as the Ga_2O_3 concentration increases, reflecting the progressive increase in bond ionicity and perturbation of the local electronic environment around silicon. (b) The progressive increase of Ga_2O_3 in the glass series leads to the emergence and gradual intensification of a band near 580 cm^{-1} , which is attributed to the formation of GaO_4 tetrahedra within the glass network. In addition, gallium incorporation modifies the local chemical environment of silicon, promoting a redshift of the main Si-O vibrational band associated with SiQ^2 species. This shift reflects the replacement of Si-O-Si linkages by Si-O-Ga bonds, which exhibit a more ionic character and a slightly longer bond length, consistent with the partial cleavage and reorganization of the original silicate network.

kit (New England Biolabs, #E7775) and sequenced on a NovaSeq 6000 (Illumina) set to 150 bp paired end (PE) sequencing parameters. FASTQ files were converted to FASTA. Reads containing unassigned nucleotides were excluded. Trim Galore was used to remove adapter sequences and reads <20 nt. Trimmed reads were aligned to the human genome (v38) using HISAT2 [18]. Transcripts were downloaded from GENCODE (v46) and Ensembl (v112). Count matrices for transcripts were created using Kallisto [19]. Differentially expressed (DE) genes were determined using the DESeq2 (v1.2.10) package in RStudio [20–24]. DE genes were selected according to \log_2 fold change ≥ 1 , $p \leq 0.05$ and false discovery rate (FDR) $< 5\%$. Pathway analysis was used to determine the biological pathways of the different genes using the KEGG database.

3. Results

3.1. Structural investigation: solid-state MAS NMR and Raman spectroscopy

The structural influence of Ga^{3+} on the 45S5-based glass network was investigated through ^{29}Si MAS NMR and Raman spectroscopy (Fig. 1). The ^{29}Si MAS NMR spectrum of the pristine 45S5 composition exhibits a broad and asymmetric resonance centered at approximately -80 ppm, which corresponds to SiQ^2 units, i.e., silicate tetrahedra linked by two bridging oxygens (BOs) and two non-bridging oxygens (NBOs) (Fig. 1a) [25]. This environment is characteristic of moderately depolymerized silicate networks typical of bioactive glasses, where NBOs are charge-balanced by Na^+ and Ca^{2+} ions (network connectivity, $\text{NC} \approx 2.1$). Upon progressive substitution of SiO_2 by Ga_2O_3 (1–5 mol%), the ^{29}Si resonance systematically shifts toward less negative chemical shifts, reaching approximately -72 ppm for the 5 mol% gallium glass [25]. This downfield displacement ($\Delta\delta \approx 8$ ppm) indicates a reduction in the electronic shielding of ^{29}Si nuclei, revealing a structural rearrangement of the silicate framework. The trend is primarily attributed

to the replacement of Si-O-Si bridges by Si-O-Ga linkages, as Ga^{3+} enters tetrahedral coordination within the network. Because Si-O-Ga bonds are slightly longer and more ionic than Si-O-Si, they decrease the electron density surrounding the Si atoms, resulting in lower shielding and a shift of the resonance to higher chemical shift values [26].

Additionally, the gradual broadening of the ^{29}Si signal with increasing gallium content suggests a growing distribution of local SiQ^n environments and enhanced structural disorder around Si sites. These features indicate that some Ga^{3+} ions behave as network formers, participating in the tetrahedral network through GaO_4^- units linked to SiO_4 tetrahedra via bridging oxygens. Such incorporation modifies the short-range topology of the glass but maintains a bioactive level preserving its ability to undergo ion exchange and surface reactivity in physiological media.

Raman spectroscopy provides complementary evidence for these structural modifications (Fig. 1b). The Raman spectrum of the unmodified 45S5 glass displays two main features: a broad band centered near 950 cm^{-1} assigned to Si-O stretching in SiQ^2 units, and a band at $\sim 560\text{ cm}^{-1}$ associated with Si-O-Si bending vibrations [27]. With the addition of Ga_2O_3 , two systematic changes occur. First, the main Si-O stretching band undergoes a gradual redshift, moving from ~ 950 to ~ 930 – 935 cm^{-1} . This shift indicates the replacement of stronger, more covalent Si-O-Si bonds by weaker, more ionic Si-O-Ga linkages, which exhibit lower bond energy and longer bond length [28]. The redshift therefore serves as vibrational evidence that Ga^{3+} occupies positions adjacent to the silicate tetrahedra, forming mixed Si-O-Ga environments that reduce the average stiffness of the network. Second, the band around 560 cm^{-1} progressively increases in intensity and develops a shoulder near 580 cm^{-1} with increasing gallium content [29]. This new feature is attributed to stretching vibrations of Ga-O bonds in tetrahedral GaO_4 units, confirming the presence of gallium in fourfold coordination. The growth of this band indicates that a significant fraction of Ga^{3+} ions is integrated as network former, rather than remaining as charge-compensating modifiers.

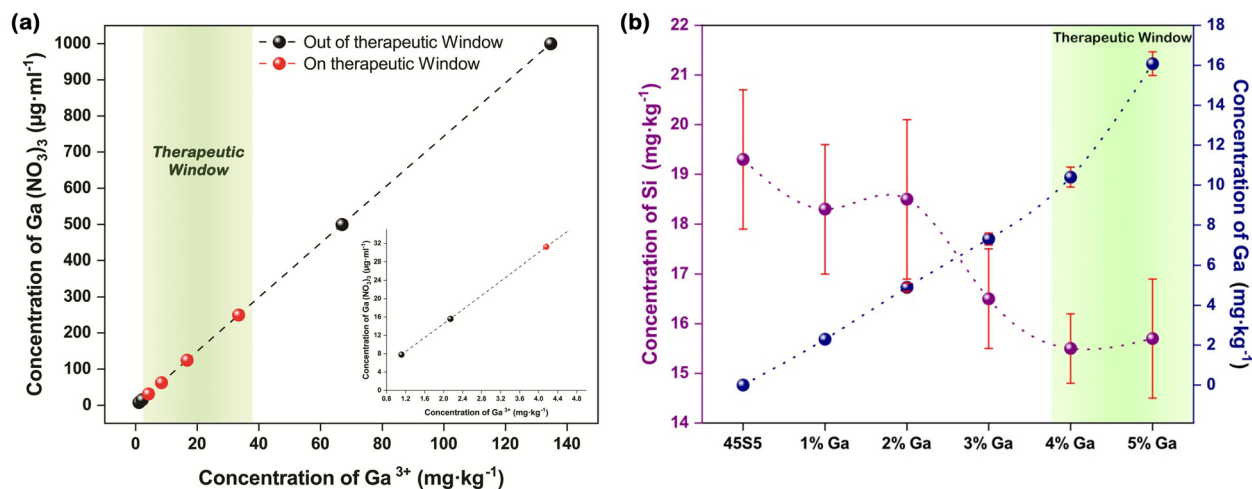


Fig. 2. Ga^{3+} -leaching from Gallium Nitrate and Ga-BGs. (a) Concentration of Ga^{3+} released by different doses of Gallium Nitrate. The small square on the bottom right corner represents a magnification of the lower concentrations. The red dots in the green zone represent the concentrations within the therapeutic window (i.e., doses that can completely kill osteosarcoma cells without affecting normal bone cells). (b) Concentration of Ga^{3+} released by bioactive glasses containing 0–5 mol% of Ga_2O_3 . The green zone represents concentrations of Ga^{3+} within the therapeutic window. The compositions containing 4 and 5 mol% of Ga_2O_3 released therapeutic amounts of Ga^{3+} . As gallium replaced Si in the glass structure, the compositions containing more Ga released less Si. Attempts to manufacture a 6 % Ga-BG proved unsuccessful as the material tended to crystallise, so no further experiments were conducted using the 6 % material.

Collectively, the ^{29}Si MAS NMR and Raman results demonstrate that Ga_2O_3 incorporation induces the progressive substitution of Si-O-Si bridges by more ionic Si-O-Ga linkages, increasing local structural disorder while maintaining the global connectivity necessary for bioactivity. Such structural reorganization is directly linked to the functional behaviour of the glasses, as the altered bond polarity and tetrahedral GaO_4 incorporation govern the dissolution dynamics and controlled release of Ga^{3+} ions, i.e., key factors for the antibacterial, antitumoral and osteogenic effects of gallium-doped bioactive glasses.

3.2. Ion-leaching from Ga-BGs

The main purpose of the bioactive glasses proposed in this study is to serve as a localized drug delivery system for anticancer and antimicrobial ions of gallium alongside with bone regenerative ions such as Ca, and P. We used ICP-OES to determine the concentrations of Ga^{3+} (in $\text{mg}\cdot\text{kg}^{-1}$) released by each dose of a serial dilution of $\text{Ga}(\text{NO}_3)_3$ used to treat the cells. Subsequently, the same method was applied to evaluate the concentrations of Ga^{3+} released by Ga-BGs to model how they compare to those of $\text{Ga}(\text{NO}_3)_3$. In addition, the concentrations of Ca, Si, and Na released by the glasses were recorded. Our results show that the concentration of Ga^{3+} presented a strong positive correlation ($\text{Ga}(\text{NO}_3)_3$ vs Ga^{3+} released, $r = 1$, $p < 0.0001$) with the tested doses of $\text{Ga}(\text{NO}_3)_3$ and that they ranged from 1.11 ± 0.03 to $134.69 \pm 0.73 \text{ mg}\cdot\text{kg}^{-1}$ of Ga^{3+} . As will be further explained in Section 3.3, a therapeutic window for gallium was observed between 31.25 and 250 μg of $\text{Ga}(\text{NO}_3)_3$, which correlates to 4.16 ± 0.13 to $33.38 \pm 0.77 \text{ mg}\cdot\text{kg}^{-1}$ of Ga^{3+} (Fig. 2a). The results for the concentration of ions leaching from Ga-containing bioactive glasses demonstrate a systematic increase in Ga^{3+} release that positively correlates to their Ga_2O_3 content (Ga_2O_3 content vs Ga^{3+} released, $r = 0.9872$, $p = 0.0002$). Furthermore, they indicated that the compositions 4 and 5 %Ga leach concentrations of gallium ions within the observed therapeutic window, which corroborates the observed results for their cytotoxicity, described in Section 3.4. (10.7 ± 0.41 and $16.08 \pm 0.59 \text{ mg}\cdot\text{kg}^{-1}$ of Ga^{3+} , respectively) (Fig. 2b). Ultimately, as the content of gallium rises in the glass composition the Si content decreases due to the reduction of SiO_2 concentration (Fig. 2b). The concentrations of Ca remained relatively stable, and Na showed a significant increase (SI.2). The concentrations of CaO and Na_2O are expected to rise as the

glass composition is renormalized to account for the reduced SiO_2 content.

3.3. Gallium nitrate therapeutic windows

The sensitivity of different types of bone cancer cells to gallium was tested and compared to the sensitivity of healthy bone cells to determine the existence of ‘therapeutic windows’, i.e., safe doses of gallium nitrate that can completely kill cancer cells without affecting healthy cells. Our results confirmed the existence of such therapeutic windows since cancerous bone cells (HOS, MNNG-HOS, 143B, Saos2, SJSA-1) were shown to be 4 to 8 times more sensitive to gallium than non-cancerous bone cells (NHOsts and hFOB) (Fig. 3). Human foetal bone cells (hFOB) were two times more sensitive to $\text{Ga}(\text{NO}_3)_3$ than normal human osteoblasts (NHOsts, extracted from elderly patient) (125 $\mu\text{g}/\text{mL}$ vs 250 $\mu\text{g}/\text{mL}$ of $\text{Ga}(\text{NO}_3)_3$ for complete cell death), which might indicate greater resistance of differentiated bone cells to gallium (Fig. 3a). The cancerous cell lines Saos2 (Fig. 3d) and SJSA-1 (Fig. 3e) were 8 times more sensitive to $\text{Ga}(\text{NO}_3)_3$ than NHOsts and 4 times more sensitive than hFOB (31.25 vs 250 /125 $\mu\text{g}/\text{mL}$ of $\text{Ga}(\text{NO}_3)_3$ for complete cell death) whereas the cell lines HOS, MNNG-HOS, and 143B were 4 times more sensitive to $\text{Ga}(\text{NO}_3)_3$ than NHOsts and 2 times more sensitive than hFOB (62.5 vs 250 /125 $\mu\text{g}/\text{mL}$ of $\text{Ga}(\text{NO}_3)_3$ for complete cell death). HOS cells exposed to 62.5 $\mu\text{g}/\text{mL}$ of $\text{Ga}(\text{NO}_3)_3$ experienced complete death after 7 days of treatment whereas MNNG-HOS (Fig. 3b) and 143B (Fig. 3c) cells died even faster, following 5 days of treatment with the same dose. Moreover, Saos2 and SJSA-1 cells also completely died in 5 days but from the lower dose of 31.25 $\mu\text{g}/\text{mL}$ of $\text{Ga}(\text{NO}_3)_3$ (Fig. 3e). Overall, these results demonstrated the existence of considerably large therapeutic windows for gallium in different osteosarcoma cell lines indicating possible dose targets for treatment.

3.4. Selective toxicity of Ga-BGs upon osteosarcoma cells

We used the observed gallium therapeutic windows as a comparative target to test whether Ga-BGs can release active gallium ions within this range and selectively kill cancerous bone cells in a similar way. For this, the same malignant and non-malignant cell lines were treated with a series of culture medium conditioned with extracts from bioactive glass powders containing 0–5 mol% of Ga_2O_3 for up to 7 days. We found that

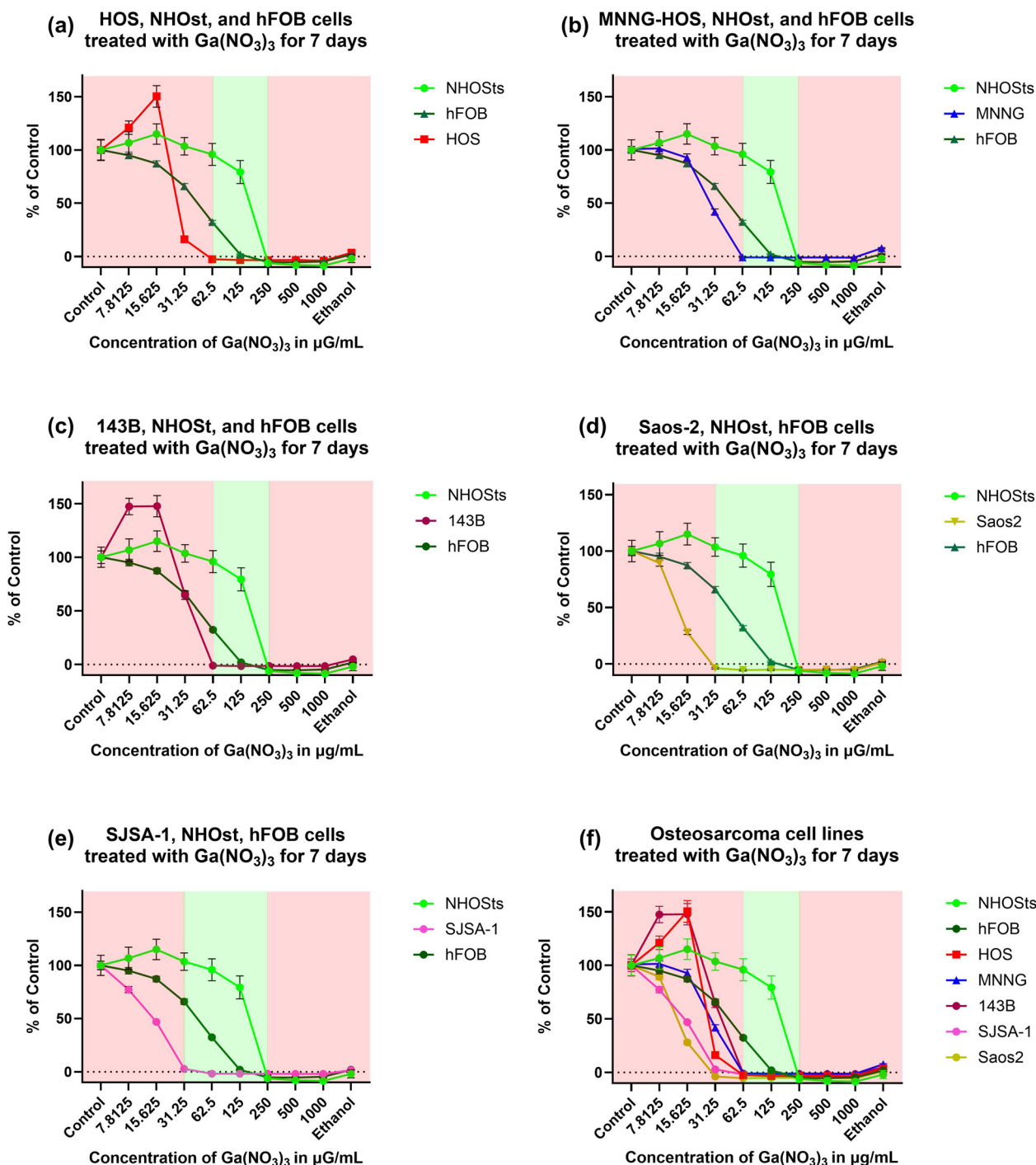


Fig. 3. Viability of different osteosarcoma cell lines treated for 7 days with different concentrations of Gallium Nitrate quantified by MTT assay and presented as percentage of control group (cells treated with their growth medium). Normal Human Osteoblasts (NHOSts) and Human Foetal Osteoblasts (hFOBs) represent healthy human bone cells and were tested in comparison to the osteosarcoma cell lines (a) HOS, (b) MNNG-HOS, (c) 143B, (d) Saos2, and (e) SJSA-1 and (f) all cell lines compared. The green zone on the graphs represents the observed ‘therapeutic windows’ for gallium, i.e., doses of Ga(NO₃)₃ which were toxic to osteosarcoma cells but safe to normal bone cells. The last graph (f) aggregates the results for all tested cell lines. Micrographs on the top right corner of each graph shows each tested cell line stained by live/dead assay (bright green = live; bright red=dead, scale bar 300 µm, 200x magnification). We observed a 4–8-fold therapeutic window for all cell lines tested. This means that osteosarcoma cancer cells are at least four times more sensitive to gallium than normal cells.

the addition of gallium into the glass promoted a temporary reduction in the viability of non-transformed bone cells (hFOBs and NHOSts) (days 3 and 5) when compared to control group. Since medium was not replaced during the 7 days of the experiment, and the dose of gallium was shown not to be enough to promote complete cell death, NHOSts recovered their levels of viability by day 7 (Fig. 4a and 4b). Supplementing

cell culture medium with 10 mg/mL of all bioactive glasses (including 0 %Ga-BG) reduced cell viability crudely by half after 7 days, showing no relationship between the content of gallium in the glass and a decline or rise in cell viability (Ga₂O₃ content vs NHOSts/hFOB Cell Viability, Day 7, $r = 0.1169/-0.7123$, $p = 0.8255/0.1123$, ns) (Fig. 4). This confirmed that the concentrations of free gallium released by the glasses

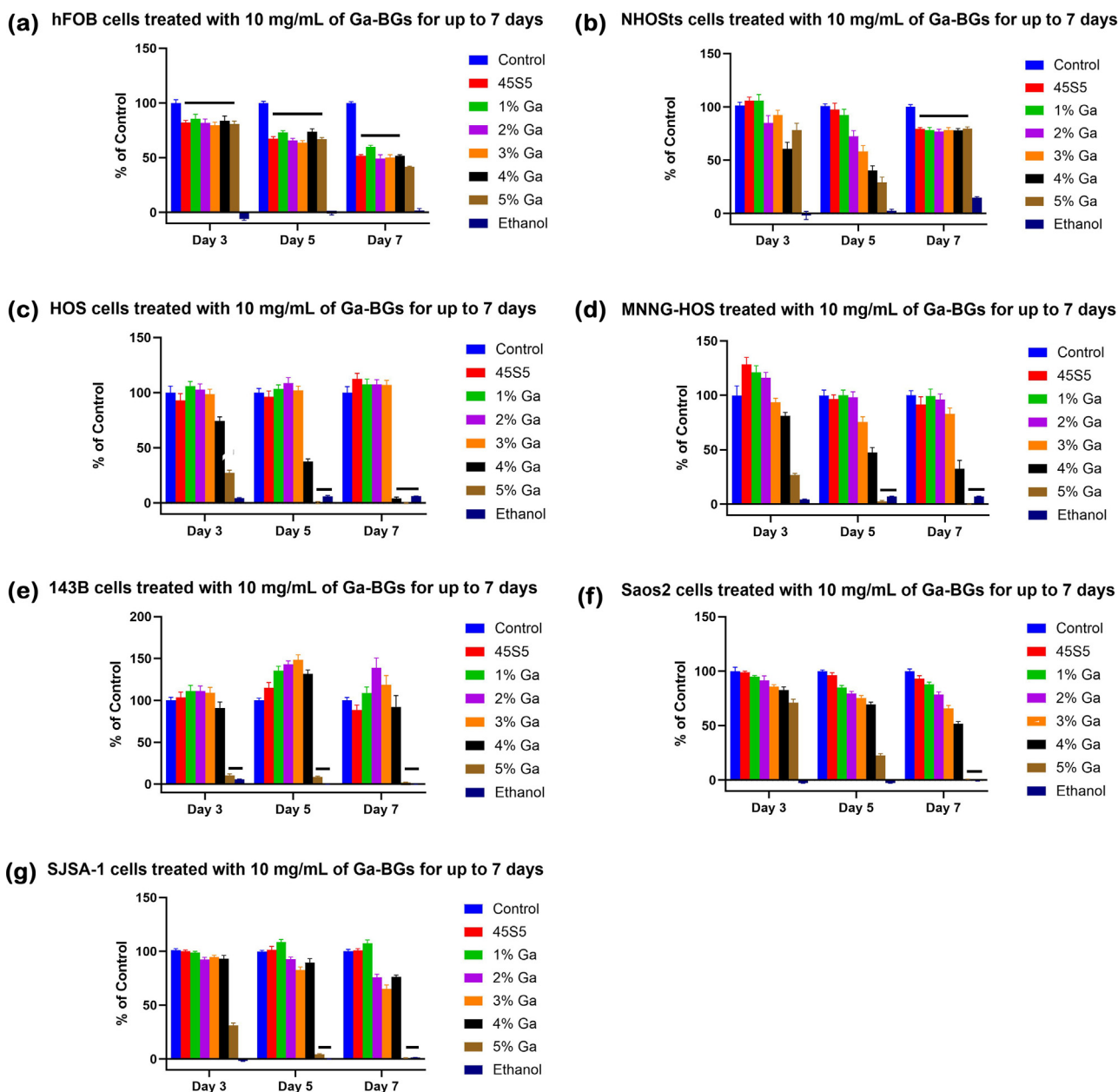


Fig. 4. Viability of different osteosarcoma cell lines treated for 7 days with bioactive glasses containing 0–5 mol% Ga_2O_3 at the concentration of 10 mg/mL quantified by MTT assay and presented as percentage of control group (cells treated with their growth medium). (a) Human Foetal Osteoblasts (hFOBs) and (b) Normal Human Osteoblast (NHOSts) represent healthy human bone cells. The (c) HOS, (d) MNNG-HOS, (e) 143B, (f) Saos2 and (g) SJSA-1 represent the different cell lines treated with bioactive glasses containing gallium. This investigation sought to determine the selective cancer-killing potential of gallium-doped glasses for primary bone cancer cells. We observed that at the concentration of 10 mg/mL the Ga-BGs powders containing 4 and 5 mol% Ga_2O_3 were able to significantly kill bone cancer cells with no effect on normal human bone cells.

fall within the therapeutic windows shown in Fig. 3. On the other hand, our results indicated that malignant bone cells are sensitive to bioactive glasses containing gallium. The composition containing 5 mol% of Ga_2O_3 promoted complete cell death of the cell lines HOS, MNNG-HOS, 143B and SJSA-1 after 5 days of treatment, whilst complete death of Saos2 was achieved after 7 days of treatment with that glass composition (Fig. 4). HOS cells were sensitive to the glass composition containing 4 mol% of Ga_2O_3 , undergoing complete cell death after 7 days of treatment (Fig. 4). These findings indicated a causative effect for the presence of gallium in the glasses with highly significant differences observed in the viability of the cancer cells treated with gallium-free bioactive glass (45S5) in comparison with bioactive glasses containing 5, 4, and in some cases, even 3 and 2 mol% of Ga_2O_3 . Therefore, these results imply

that the concentrations of free gallium released by the 4 and 5 %Ga-BGs also fall within the therapeutic windows shown in Fig. 3. Altogether, our observations confirm that bioactive glasses containing 4–5 mol% of Ga_2O_3 release active gallium ions within therapeutic windows and may constitute an effective drug delivery system for localized delivery of anticancer ions of gallium.

3.5. Apoptosis-inducing potential of Ga-BGs

To evaluate the potential of 5 %Ga-BG to stimulate apoptosis in malignant (HOS, MNNG-HOS, 143B, SJSA-1, Saos2) and non-transformed (hFOB) cell lines, cells were treated with glass-conditioned (at 10 mg/mL) medium for a duration of 7 days and assessed by means

of caspase 3/7 assay. Results demonstrated absence of caspase activation in hFOB cells treated with 5 %Ga-BG for 7 days (Fig. 5). On the other hand, all cancer cell lines presented substantial caspase activity when treated with 5 %Ga-BG for 7 days, suggesting that the cell death observed in the viability experiments may be following the apoptotic pathway (Fig. 5).

3.6. Mechanism of action by RNA sequencing (RNA-seq)

While RNA-seq is not a direct genotoxicity test similar to traditional assays (e.g. Ames test, micronucleus assay, etc.), it can be a valuable tool in genotoxicity studies by providing insights into the molecular mechanisms and biological responses to new therapeutic agents. Thus, we used RNA-seq as a hypothesis-free strategy to identify differentially expressed (DE) genes and affected cellular pathways in response to $\text{Ga}(\text{NO}_3)_3$. This strategy was used to support a mechanistic justification for the observed therapeutic window for $\text{Ga}(\text{NO}_3)_3$ and the selective toxicity of Ga-BGs upon metastatic osteosarcoma cells (143B cell line). This analysis revealed a distinct and extensive transcriptomic reprogramming in 143B cells treated with 62 $\mu\text{g}/\text{mL}$ $\text{Ga}(\text{NO}_3)_3$. This treatment resulted in the DE of 609 genes (Fig. 6a), indicating a broad and significant cellular response to gallium nitrate. In contrast, normal bone cells (hFOB cell line) treated under identical conditions showed a remarkably limited set of 6 DE genes, emphasizing the remarkable selective impact of gallium towards malignant cells (Fig. 6b). This striking disparity in gene expression profiles provides a molecular foundation for the observed therapeutic window. A list of all up- and downregulated genes in 143B and hFOB cells and their primary biological functions as well as heatmaps and GO analysis can be found in SI.3. The transcriptomic profile of bone cancer cells treated with gallium nitrate reveals a multi-faceted attack on key hallmarks of cancer, primarily through the disruption of iron metabolism, leading to increased oxidative stress, induction of cell death pathways, and suppression of oncogenic and metastatic signalling.

3.7. Antibacterial activity of Ga-BGs

Considerable evidence suggests that gallium has inhibitory effect against selected strains of bacteria [30–32]. We evaluated the antibacterial potential of a series of doses of $\text{Ga}(\text{NO}_3)_3$ and of different concentrations (w/v) of 5 % Ga-BG by determining their minimum inhibitory concentration (MIC) against *P. aeruginosa*, responsible for significant hospital-acquired infection [33,34]. Results indicated that 62 $\mu\text{g}/\text{mL}$ $\text{Ga}(\text{NO}_3)_3$ starts to inhibit bacterial growth and at 125 $\mu\text{g}/\text{mL}$ it completely inhibits growth. These results confirmed that concentrations of $\text{Ga}(\text{NO}_3)_3$ within the pre-determined therapeutic windows (shown in Section 3.3) can, in addition to selectively kill bone cancer cells, prevent growth of the gram-negative bacteria *P. aeruginosa*. Since the tested concentration of bioactive glass in cell culture medium used to treat cells was of 10 mg/mL we can conclude that it falls within the bacterial inhibitory range observed in this experiment. Altogether, these findings indicate that *P. aeruginosa* are sensitive to gallium and that the glass composition 5 % Ga-BG can inhibit their growth, thus, aiding in the prevention implant-site contamination (Fig. 7).

4. Discussion

This work sought to determine the existence of therapeutic windows for gallium in several cell lines of osteosarcoma and the efficacy of gallium-containing bioactive glasses (Ga-BGs) to release gallium ions within these pre-determined therapeutic windows to selectively kill bone cancer cells. In addition, we sought to determine, for the first time, the intricate intracellular molecular mechanisms of selective cell death induced by gallium upon osteosarcoma cells (143B) which are known to be prone to metastasize. Finally, we evaluated the antibacterial potential of 5 % Ga-BG upon *P. aeruginosa*. Our results confirmed the existence of 4–8-fold therapeutic windows for gallium for different bone cancer cell

lines and that 4 and 5 % Ga-BGs release concentrations of Ga ions within the therapeutic range and can selectively kill cancer cells with minimum toxicity upon healthy bone cell lines and 125 $\mu\text{g}/\text{mL}$ of $\text{Ga}(\text{NO}_3)_3$ and 10 mg/mL 5 %Ga-BG can inhibit growth of *P. aeruginosa*.

4.1. Gallium promotes cellular crisis in osteosarcoma via multi-pronged molecular attack

The incorporation of gallium into bioactive glasses proposed in the present work aimed to overcome the limitation of conventional drug administration routes (e.g. oral, intravenous) in delivering adequate doses of gallium to bone tissue whilst simultaneously promoting rapid bone repair. When taken orally as a salt, the actual dose of gallium reaching the bone tumours was shown to be very low [13]. An alternative method is to administer $\text{Ga}(\text{NO}_3)_3$ via continuous infusion for 5–7 days, which is both logistically challenging and has been shown to cause nephrotoxicity in some patients when bolus doses were used [35]. The literature on gallium containing bioactive materials has recently been comprehensively reviewed, showcasing a wide range of compositions proposed for osteogenic, antibacterial and anticancer applications [31]. Our dissolution results demonstrated that our Ga-BGs could function as localized systems for delivery of adequate amounts of gallium, especially the compositions containing 4 and 5 mol% of Ga_2O_3 (Fig. 2).

Much of the explanation for the selective toxicity of Ga comes from the similarity between its coordination chemistries (ionic radii, ionization potential, electronegativity, etc.) and those of Fe^{3+} that allows for Ga^{3+} to bind to the two metal sites of the predominantly iron-carrier protein Transferrin (Tf), present in blood plasma and Foetal Bovine Serum in cell culture medium [11,35]. In addition to these similarities, some important differences may explain gallium selective toxicity to cancer cells. The most important of these differences is the fact that whereas Fe^{3+} can be easily reduced to Fe^{2+} (and then reoxidized), Ga^{3+} is almost irreducible in physiological conditions, which appears to prevent it from entering Fe^{2+} binding molecules such as heme and cytochrome, and to prevent it from participating in redox reactions [35,36]. This means that Ga^{3+} can bind to Transferrin ligands but cannot perform the same functions of iron, therefore, leading to Fe depletion and disruption of Fe-dependent molecular pathways, interfering with iron metabolism and leading to excessive oxidative stress. Our transcriptome data demonstrate the upregulation of numerous genes involved in managing oxidative stress and iron homeostasis including *HMOX1*, *GCLM*, *GPX3*, *NQO1*, *TXNRD1*, *SLC7A11*, *CHAC1*, *SESN2*, *GSR*, *FTH1*, *SQSTM1*, and *NDRG1* (Fig. 6a) corroborating the notion that the excess of gallium within bone cancer cells disrupts iron metabolism by impairing iron-dependent enzymes and the synthesis of iron-sulfur clusters, which are essential for DNA synthesis and repair [37]. The upregulation of *HMOX1* (heme oxygenase-1), *NQO1* (NAD(P)H quinone dehydrogenase 1), *GCLM* (glutamate-cysteine ligase modifier subunit), *GPX3* (glutathione peroxidase 3), *TXNRD1* (thioredoxin reductase 1), and *GSR* (glutathione reductase) suggests activation of the NRF2-mediated oxidative stress response pathway [38] (Fig. 6a). NRF2 is a transcription factor that regulates heme and iron metabolism through the transcriptional upregulation of multiple genes, including heme oxygenase 1 (*HMOX1*), which was seven-fold upregulated in 143B cells (SI.3). NRF2 is recognized as a master regulator of antioxidant and detoxifying enzymes, and its activation represents a fundamental cellular defence mechanism against increased reactive oxygen species (ROS) and cellular damage [38]. The strong upregulation of NRF2-target genes suggests that the iron dysregulation caused by gallium is leading to significant oxidative stress in the cells leading them to a state of cellular crisis [39,40]. The elevated expression of *GCLM* (a crucial enzyme in glutathione synthesis) and *SLC7A11* (a subunit of the cystine/glutamate antiporter, responsible for cystine uptake, which is then converted to cysteine for GSH synthesis) points to an attempt by the cancer cells to bolster their glutathione antioxidant system [39]. Similarly, the increased levels of *TXNRD1* and *GSR* signify enhanced activity of the thioredoxin and glutathione re-

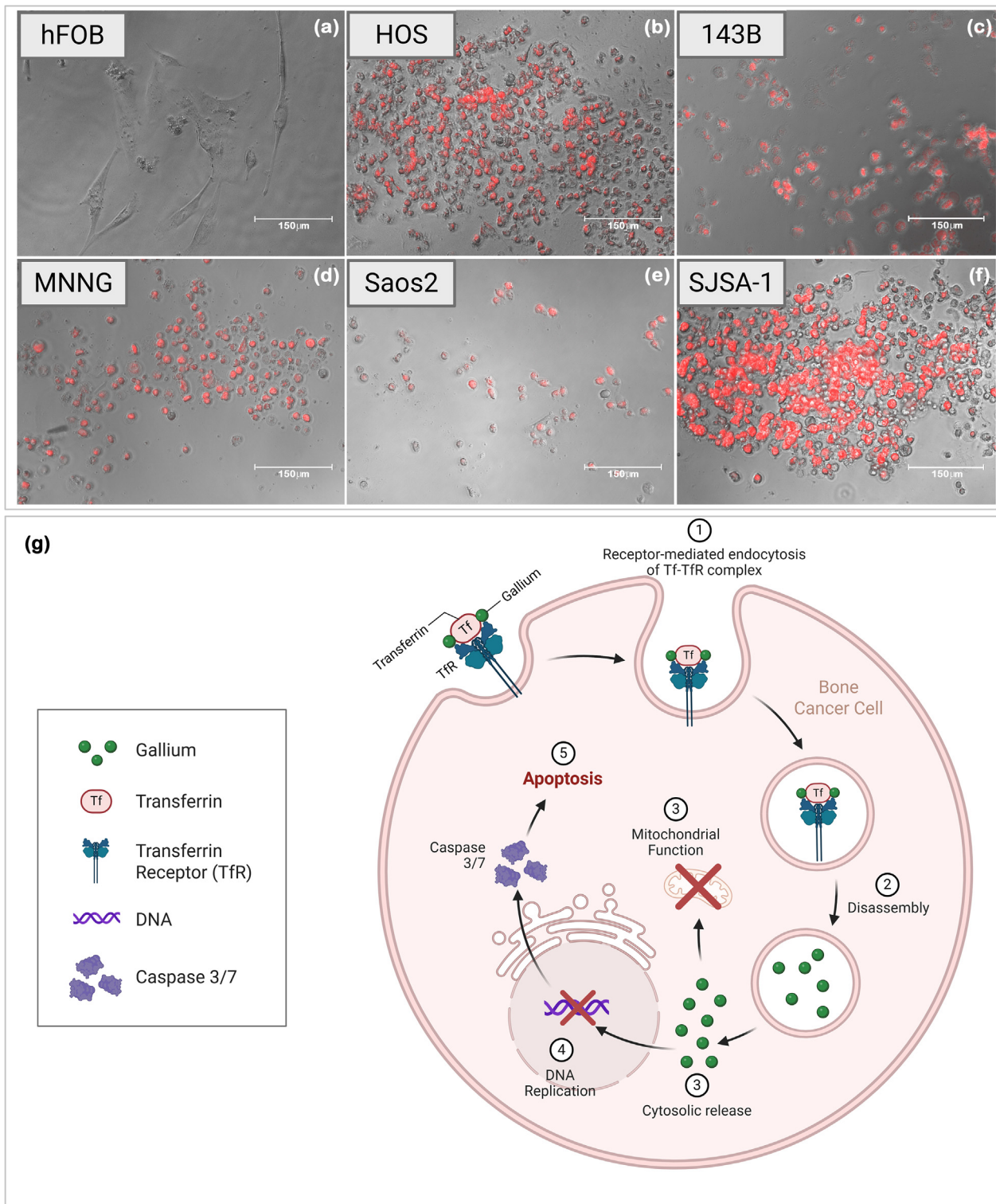


Fig. 5. Caspase 3/7 activity in different bone cell lines treated for 7 days with a bioactive glass containing 5 mol% Ga₂O₃ at the concentration of 10 mg/mL. In caspase 3/7 assay images, the nuclei of apoptotic cells are shown in bright red. (a) Human Foetal Osteoblasts (hFOB) represent healthy human bone cells. (b) HOS, (c) 143B, (d) MNNG-HOS, (e) Saos2 and (f) SJSA-1 represent osteosarcoma cells. Cancer cell lines presented substantial caspase activity when treated with 5 %Ga-BGs whereas no caspase 3/7 activation was observed in the healthy cells. (g) Schematic representation of proposed mechanism of action of Ga³⁺ in promoting cellular apoptosis. Transferrin ligands carrying Ga³⁺ attach to TfR and are internalized to cell by endocytosis (1), the Tf-TfR complex disassembles (2) and release Ga³⁺ in the cytosol (3). Ga ions promote excessive oxidative stress, compromise mitochondrial functions (3) and DNA synthesis (4) leading the cell to state of crises, activating the apoptotic pathway (5). Expression of executioner caspases 3/7 represent the hallmark of apoptotic response.

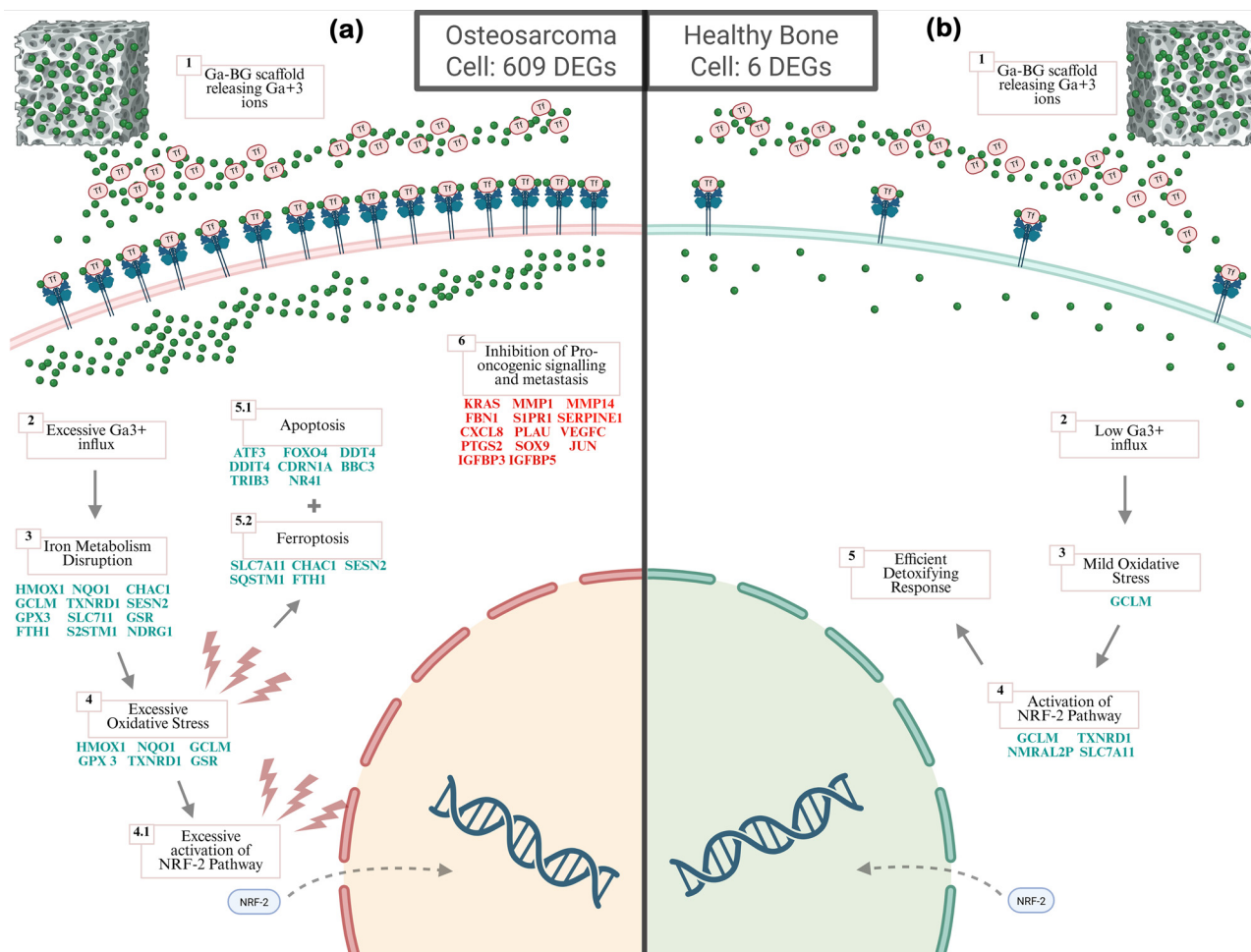


Fig. 6. High-level overview of the sequencing / mechanism of action of Ga³⁺ upon osteosarcoma cells (a) and healthy bone cells (b). Exposure to gallium ions stimulated 609 DEGs in cancer cells suggesting they were under immense pressure, attempting to cope with an overwhelming assault to their cellular machinery, particularly their iron-dependent processes. Excessive oxidative stress was observed which led to over activation of detoxifying NRF2 pathway, which ultimately proved inefficient. A multi-pronged molecular attack on key hallmarks of cancer resulting in cell death by ferroptosis and apoptosis. In addition, gallium has inhibited expression of pro-oncogenic genes related to migration, invasion, angiogenesis, inflammation, as well as cellular genes related to growth and differentiation (a). On the other hand, the same therapy stimulated only 6 DEGs in healthy bone cells. In those cells, Ga³⁺ promoted only mild oxidative stress. The NRF2 pathway activation was effective in detoxifying the cell and prevent cellular death (b). The differential Ga³⁺ cell influx is believed to be related to a greater expression of Tf-receptors by cancer cells than in normal cells.

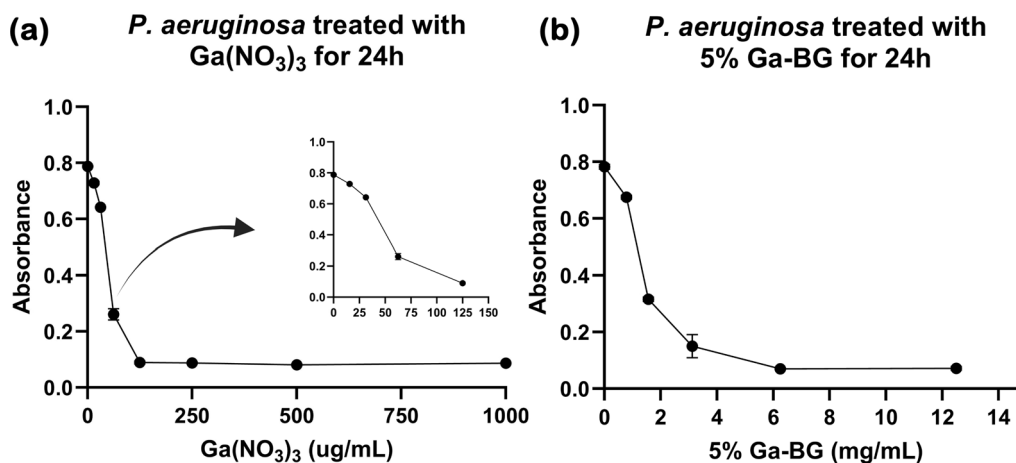


Fig. 7. Antibiotic activity of gallium nitrate (Ga(NO₃)₃) and 5% Ga-BG upon *P.aeruginosa*. (a) *P.aeruginosa* cells treated with a serial dilution of gallium nitrate for 24 h. The inset represents a magnification of the low concentrations. A dose of 62µg/mL of Ga(NO₃)₃ starts to affect bacterial growth and at 125 ug/mL the treatment can completely inhibit it. (b) *P.aeruginosa* cells treated a serial dilution of 5 %Ga-BG in broth for 24 h. Concentrations above 6 mg/mL of 5 %Ga-BG were shown to completely inhibit bacterial cell growth. Therefore, since the tested concentration of bioactive glass in cell culture medium used to treat cells in all other biological experiments was of 10 mg/mL we can conclude that it falls within the bacterial inhibitory range observed in this experiment.

ductase systems, respectively, both of which are vital for maintaining cellular redox balance and detoxifying harmful intermediates [40]. This widespread activation of antioxidant defences suggests that gallium is effectively overwhelming the cancer cells' capacity to maintain redox homeostasis. Despite all efforts, the antioxidant cellular response was not enough to reestablish homeostasis, leading to programmed cell death. The upregulation of both pro-apoptotic and ferroptosis-related genes may indicate a multi-pronged attack to cancer cells that may render it harder for cells to develop drug resistance mechanisms against gallium (Fig. 6a). Results from a previous study that investigated the effect of gallium(III) Tris(acetyl-pyrazolonate) complexes on a range of cancer cell types corroborates this idea. The authors of that study concluded that gallium complexes acted on different and multiple cellular targets to induce ferroptosis in cancer cells via dysregulation of cell redox homeostasis and inhibition of the mevalonate pathway [41]. Our RNA-seq data combined with apoptosis assays suggest that gallium toxicity is directly linked to the induction of programmed cell death (Fig. 6a). Sequencing data shows the upregulation of several genes associated with programmed cell death and stress responses, including *ATF3*, *FOXO4*, *DDIT4*, *CDKN1A*, *BBC3*, *TRIB3*, and *NR4A1*. *ATF3* (Activating Transcription Factor 3) is a key stress-inducible transcription factor frequently overexpressed in various cancer types. Under stress conditions, *ATF3* is known to activate pro-apoptotic genes, including *BBC3* (PUMA) [42]. The upregulation of *BBC3* (PUMA) is particularly significant, as it is a direct transcriptional target of TP53 and a potent pro-apoptotic mediator, playing a crucial role in TP53-mediated cell death. Its increased expression is a strong indicator of apoptosis pathway activation [42]. In fact, our results from caspase 3/7 assay demonstrate increased activity of these executioner apoptotic enzymes in bone cancer cells treated with 4 and 5 % Ga-BGs (Fig. 5).

In contrast with osteosarcoma cells, sequencing data from normal bone cells (hFOB) treated with 62 µg/mL Ga(NO₃)₃ for 36 h revealed a very limited set of upregulated genes: *GCLM*, *NMRAL2P*, *SLC7A11*, and *TXNRD1* (Fig. 6b). This minimal yet focused response is highly significant. Similar to the response observed in cancer cells, the NRF2-mediated antioxidant and stress response pathway were activated to detoxify reactive species and maintaining cellular redox homeostasis. However, unlike cancer cells, healthy cells successfully manage the trauma, preventing widespread cellular damage and maintaining viability. The difference in the number and scope of DE genes between healthy and cancer cells is the direct molecular basis of the observed therapeutic window (Fig. 6). Normal cells primarily activate a focused, robust antioxidant defence (NRF2 pathway), indicating they are inherently equipped to handle the gallium-induced stress without succumbing to toxicity. This fact may explain the toxicity of relatively low doses of gallium nitrate and of 10 mg/mL of Ga-BGs upon the tested bone cancer cell lines (HOS, MNNG-HOS, 143B, Saos2, SJSA-1) that we found in our experiments.

4.2. Gallium inhibits oncogenic and metastatic genes in osteosarcoma cells

In addition to promoting excessive oxidative stress and inducing cell death, the treatment with gallium nitrate was shown to downregulate a series of oncogenic and metastatic genes linked to cell proliferation, invasion, angiogenesis, and epithelial-mesenchymal transition (EMT) such as *KRAS*, *MMP1*, *MMP14*, *PTGS2*, *VEGFC*, *FBN1*, *SOX9*, *JUN*, *IGFBP3*, *IGFBP5*, *S1PR1*, *SERPINE1*, *CXCL8*, and *PLAU* (Fig. 6a, SI.3). *KRAS* is a prominent oncogene frequently mutated and activated in various cancers, including osteosarcoma [43,44]. Reducing the activity of *KRAS* in osteosarcoma cells (MG-63, KHOS, U-2OS, and Saos2) has been shown to inhibit cell migration and invasion *in vitro* and *in vivo* by inhibiting *MMP1*, *MMP3* and *MMP9* via an IL17 signal-dependent manner [43]. The potential suppression of invasion and metastasis following treatment with gallium is further supported by the downregulation of *MMP1* and *MMP14*. These enzymes are crucial for the degradation of the extracellular matrix (ECM), facilitating cell migration and invasion, and

are highly associated with osteosarcoma metastasis [2,45–48]. Moreover, upregulation of *MMP14* expression is related to epithelial- and endothelial-to-mesenchymal transition (EMT), where epithelial or endothelial cells acquire mesenchymal features, which commonly happens to metastatic osteosarcoma cells [2,45,47]. Other genes like *FBN1* (Fibrillin 1) [49], *S1PR1* (Sphingosine-1-phosphate receptor 1), *SERPINE1* (Plasminogen Activator Inhibitor 1, PAI-1) [50,51], *CXCL8* (Interleukin-8) [52–54], and *PLAU* (Urokinase Plasminogen Activator) [55,56] are all implicated in various aspects of cancer progression, including invasion, metastasis, angiogenesis, and inflammation. The inhibition of angiogenesis and inflammation is further supported by the downregulation of *PTGS2* (Cyclooxygenase-2, COX-2) and *VEGFC*. *VEGFC* is a crucial factor promoting tumour angiogenesis and lymphangiogenesis, both essential for tumour growth and metastatic dissemination and was found to be associated with poor overall survival in osteosarcoma [57]. Finally, the modulation of growth and differentiation is indicated by the downregulation of *SOX9*, *JUN*, *IGFBP3*, and *IGFBP5* [58,59]. *SOX9* is a key transcriptional regulator involved in developmental processes, overexpressed locally and in the circulation in bone cancer, and linked to EMT, stem cell phenotypes, and drug resistance. It has also demonstrated positive correlation with tumour severity, malignancy, and size [60]. Concomitantly, *IGFBP-3* has been shown to facilitate *VCAM1* production and cell migration in human osteosarcoma via the *PI3K*, *Akt* and *AP-1* signalling pathways [58]. These findings provide a robust foundation for understanding the molecular basis of gallium's anticancer activity and its selective nature, indicating that gallium: (a) disrupts iron metabolism; (b) induces oxidative stress; (c) leads to cell death via ferroptosis and apoptosis; (d) inhibits pro-oncogenic and metastatic genes. This supports the development of gallium-containing bioactive glasses as a promising therapeutic approach for bone tumour treatment (Fig. 6).

4.3. Antibacterial activity of Ga-BGs

Infection control is critical for immunocompromised patients as their weakened defences make them highly susceptible to severe, often fatal infections from environmental and opportunistic pathogens. Doses of gallium nitrate within the therapeutic window also presented inhibitory effect upon gram-negative bacteria *P. aeruginosa*, a common environmental and hospital pathogen that frequently exhibits intrinsic and acquired multidrug resistance, making resulting infections exceptionally difficult to treat compared to many other bacteria [33,34]. Our results corroborate previous investigations of other gallium compounds [11,13,30,31,35,36,61–63]. In microorganisms, gallium was shown to interfere with survival and growth by exchanging for iron in siderophores [63]. In the case of *P. aeruginosa*, the siderophore pyochelin has been shown to be responsible for transporting gallium [63]. As with cancer cells, gallium cannot be utilized for essential iron-catalysed reactions, thus, leading to the death of the organism. A previous investigation combined antibacterial nanospheres of elemental gallium (16 wt.%) with bioactive hydroxyapatite nanorods (84 wt.%) to prepare nanocomposites with potential antimicrobial activity. The produced nanocomposite exhibited superior antibacterial properties against *P. aeruginosa* and lower *in vitro* cytotoxicity for human lung fibroblasts IMR-90 and mouse fibroblasts L929 when compared to a nanocomposite of hydroxyapatite and silver nanoparticles, which suggests that such composite can promote prevention of implantation-induced infections that are frequently caused by *P. aeruginosa* [64]. Goss and colleagues tested the potential of gallium as an antibacterial treatment both in a mice model and in a phase I clinical trial [65]. First, they showed that a single parenteral dose of gallium administered 3 or 12 h after infection in mice with *P. aeruginosa* lung infection was enough to reduce lung and blood *P. aeruginosa* counts and increase survival. Secondly, they tested intravenous gallium administration in patients with cystic fibrosis and chronic *P. aeruginosa* lung infections in a pilot phase Ib study involving 20 patients. They observed that a single 5-day intravenous infusion of gallium reduced sputum *P. aeruginosa* density and significantly increased

lung function at 14 and 28 days, without signs of any serious adverse events [65]. Therefore, the results observed in the present study corroborate previous findings demonstrating that gallium-containing materials present antibacterial activity and can aid in preventing intra and post-operative infections.

Taken together, the biological results indicate that bioactive glasses containing 4–5 mol% Ga₂O₃ represent the optimal compositions for therapeutic performance, with the 5 % Ga-BG formulation emerging as the most effective candidate. The observed convergence of selective anticancer activity, antibacterial performance, and minimal cytotoxicity toward healthy cells highlights the therapeutic relevance of the 5 % Ga-BG composition. From a materials design perspective, this composition appears to provide the most favourable balance between gallium incorporation within the glass network and controlled ion release, ensuring sufficient Ga³⁺ delivery to disrupt iron-dependent pathways in cancer cells while remaining within a biologically safe range for normal bone cells.

5. Conclusions

We demonstrated the existence of large therapeutic windows for gallium in different cell lines of osteosarcoma and that bioactive glasses containing 4–5 mol% of Ga₂O₃ release active gallium ions within the therapeutic windows and can selectively kill bone cancer cells within seven days of treatment. The selective toxicity of gallium to osteosarcoma cells was shown to be caused by a multi-pronged molecular attack on key hallmarks of cancer, primarily through the disruption of iron metabolism, leading to increased oxidative stress, induction of cell death pathways, and suppression of oncogenic and metastatic signalling. In addition, gallium nitrate and 5 %Ga-BG were shown to present inhibitory effect upon gram-negative bacteria *P. aeruginosa*. Altogether, our results indicate that Ga-containing bioactive glasses constitute an ideal biomaterial for the development of multi-functional scaffolds for the treatment of osteosarcoma promoting localized delivery of anticancer, antibiotic and bone regenerative ions that can prevent implant-site contamination, cancer re-occurrence and enhance bone regeneration, leading to superior treatment outcomes.

Data availability

All available data are included in this article and its supplementary files or are available from the corresponding author upon request. Raw sequencing files are deposited in the NCBI Sequence Read Archive (SRA) and publicly available under accession PRJNA1335238.

Funding sources

This work was supported by [Bone Cancer Research Trust \(BCRT\) \[BCRT7921\]](#); [Royal Orthopaedic Hospital Charity \[#135\]](#); [Orthopaedic Research UK \[ORUK:594\]](#), [RAEng/Leverhulme Trust Senior Research Fellowship \[Developing bioactive glasses for bone cancer therapy\]](#), [Paediatric Cancer Research programme at UEA](#), [Brazilian National Council for Scientific and Technological Development \(CNPq\) \[444922/2024-5\]](#) and [Sao Paulo Research Foundation \(FAPESP\) \[2022/03247-6, 2023/07910-4, and 2025/01038-9\]](#).

Declaration of competing interest

The authors declare that they have no known competing financial interests or personal relationships that could have appeared to influence the work reported in this paper.

CRedit authorship contribution statement

Lucas Pereira Lopes de Souza: Writing – review & editing, Writing – original draft, Visualization, Validation, Supervision, Resources,

Project administration, Methodology, Investigation, Funding acquisition, Formal analysis, Data curation, Conceptualization. **Joao Henrique Lopes:** Writing – review & editing, Writing – original draft, Visualization, Validation, Investigation, Funding acquisition, Formal analysis, Data curation. **Luis Felipe Moreira Oliveira:** Writing – review & editing, Writing – original draft, Visualization, Validation, Investigation, Formal analysis, Data curation. **Farah Naz Safdar Raja:** Writing – review & editing, Investigation, Formal analysis, Data curation. **Archana Singh:** Software, Investigation, Formal analysis, Data curation. **Shirin Hanaei:** Writing – review & editing. **Darrell Green:** Writing – review & editing, Writing – original draft, Visualization, Validation, Investigation, Formal analysis, Data curation. **Adrian Gardner:** Writing – review & editing, Funding acquisition, Conceptualization. **Jonathan Stevenson:** Writing – review & editing, Funding acquisition, Conceptualization. **Richard Alan Martin:** Writing – review & editing, Writing – original draft, Visualization, Validation, Funding acquisition, Formal analysis, Data curation, Conceptualization.

Acknowledgments

We thank our former placement students Eiman Hasan, Mariella Gonsalves and Blake Yexley for maintaining the instruments in the Dubrowsky Laboratory and for running some experiments. The authors are grateful to Bone Cancer Research Trust (BCRT) for facilitating consultation meetings with its Patient & Public Involvement Panel (PPIP), which gave us great insights about patients' views of our project. Biorender was used in the artwork presented in this article.

Supplementary materials

Supplementary material associated with this article can be found, in the online version, at [doi:10.1016/j.engreg.2026.05.001](https://doi.org/10.1016/j.engreg.2026.05.001).

References

- [1] F. Jafari, S. Javdansirat, S. Sanaie, A. Naseri, A. Shamekh, D. Rostamzadeh, S. Dolati, Osteosarcoma: a comprehensive review of management and treatment strategies, *Ann. Diagn. Pathol.* 49 (2020) 151654.
- [2] E.C. Bull, A. Singh, A.M. Harden, K. Soanes, H. Habash, L. Toracchio, M. Carrabotta, C. Schreck, K.M. Shah, P.V. Riestra, M. Chantoiseau, M.E.M. Da Costa, G. Moquin-Beaudry, P. Pantziarka, E.A. Essiet, C. Gerrand, A. Gartland, L. Bojmar, A. Fahlgren, A. Marchais, E. Papakonstantinou, E.M. Tomazou, D. Surdez, D. Heymann, F. Cidre-Aranaz, O. Fromigie, P.A. Meyers, R. Nagarajan, R.L. Randall, T.G.P. Grünwald, K. Scotlandi, M. Nathrath, D. Green, Targeting metastasis in paediatric bone sarcomas, *Mol. Cancer* 24 (2025) 153.
- [3] S. Smeland, S.S. Bielack, J. Whelan, M. Bernstein, P. Hogendoorn, M.D. Krailo, R. Gorlick, K.A. Janeway, F.C. Ingleby, J. Anninga, I. Antal, C. Arndt, K.L.B. Brown, T. Butterfass-Bahloul, G. Calaminus, M. Capra, C. Dhooge, M. Eriksson, A.M. Flanagan, G. Friedel, M.C. Gebhardt, H. Gelderblom, R. Goldsby, H.E. Grier, R. Grimer, D.S. Hawkins, S. Hecker-Nolting, K. Sundby Hall, M.S. Isakoff, G. Jovic, T. Kühne, L. Kager, T. von Kalle, E. Kabickova, S. Lang, C.C. Lau, P.J. Leavey, S.L. Lessnick, L. Mascarenhas, R. Mayer-Steinacker, P.A. Meyers, R. Nagarajan, R.L. Randall, P. Reichardt, M. Renard, C. Rechnitzer, C.L. Schwartz, S. Strauss, L. Teot, B. Timmermann, M.R. Sydes, N. Marina, Survival and prognosis with osteosarcoma: outcomes in > 2000 patients in the EURAMOS-1 (European and American osteosarcoma study) cohort, *Eur. J. Cancer* 109 (2019) 36–50.
- [4] L. Ambrosio, M.G. Raucci, G. Vadalà, L. Ambrosio, R. Papalia, V. Denaro, Innovative biomaterials for the treatment of bone cancer, *Int. J. Mol. Sci.* 22 (15) (2021) 8214.
- [5] J. Liao, R. Han, Y. Wu, Z. Qian, Review of a new bone tumor therapy strategy based on bifunctional biomaterials, *Bone Res* 9 (2021) 18.
- [6] N. Papalexis, A. Parmeggiani, G. Peta, P. Spinnato, M. Miceli, G. Facchini, Minimally invasive interventional procedures for metastatic bone disease: a comprehensive review, *Curr. Oncol.* 29 (6) (2022) 4155–4177.
- [7] F. Migliorini, N. Maffulli, A. Trivellas, J. Eschweiler, M. Tingart, A. Driessen, Bone metastases: a comprehensive review of the literature, *Mol. Biol. Rep.* 47 (8) (2020) 6337–6345.
- [8] D. Greenspan, Bioglass at 50 – a look at Larry Hench's legacy and bioactive materials, *5 (1)* (2019) 178–184.
- [9] M.M. Hart, R.H. Adamson, Antitumor activity and toxicity of salts of inorganic group IIIa metals: aluminum, gallium, indium, and thallium, *Proc. Natl. Acad. Sci.* 68 (7) (1971) 1623–1626.
- [10] E.M. Bomhard, The toxicology of gallium oxide in comparison with gallium arsenide and indium oxide, *Env. Toxicol. Pharmacol.* 80 (2020) 103437.
- [11] W. Sun, M. Qi, S. Cheng, C. Li, B. Dong, L. Wang, Gallium and gallium compounds: new insights into the “Trojan horse” strategy in medical applications, *Mater. Des.* 227 (2023) 111704.

- [12] C.R. Chitambar, Medical applications and toxicities of gallium compounds, *Int. J. Env. Res. Publ. Health*. 7 (5) (2010) 2337–2361.
- [13] P. Coltery, B. Keppler, C. Madoulet, B. Desoize, Gallium in cancer treatment, *Crit. Rev. Oncol. Hematol.* 42 (3) (2002) 283–296.
- [14] S.B. Hanaei, R.C. Murugesan, L.P. Souza, J.I. Cadiz-Miranda, L. Jeys, I.B. Wall, R.A. Martin, Multifunctional gallium doped bioactive glasses: a targeted delivery for antineoplastic agents and tissue repair against osteosarcoma, *Biomed. Mater.* 19 (6) (2024) 065008.
- [15] K.S. Rana, L.P. Souza, M.A. Isaacs, F.N.S. Raja, A.P. Morrell, R.A. Martin, Development and characterization of gallium-doped bioactive glasses for potential bone cancer applications, *ACS. Biomater. Sci. Eng.* 3 (12) (2017) 3425–3432.
- [16] L. Souza, F.V. Ferreira, J.H. Lopes, J.A. Camilli, R.A. Martin, Cancer inhibition and in vivo osteointegration and compatibility of gallium-doped bioactive glasses for osteosarcoma applications, *ACS. Appl. Mater. Interfaces*. 14 (40) (2022) 45156–45166.
- [17] L.L. Hench, The story of Bioglass, *Mater. Sci. Mater. Med.* 17 (2006) 967–978.
- [18] M. Pertea, D. Kim, G.M. Pertea, J.T. Leek, S.L. Salzberg, Transcript-level expression analysis of RNA-seq experiments with HISAT, StringTie and Ballgown, *Nat. Protoc.* 11 (2016) 1650–1667.
- [19] N.L. Bray, H. Pimentel, P. Melsted, L. Pachter, Near-optimal probabilistic RNA-seq quantification, *Nat. Biotechnol.* 34 (2016) 525–527.
- [20] S. Llana-Lago, W.D. Fraser, D. Green, Bayesian unsupervised clustering identifies clinically relevant osteosarcoma subtypes, *Br. Bioinform.* 26 (1) (2025) bbae665.
- [21] L. Tattersall, K.M. Shah, D.L. Lath, A. Singh, J.M. Down, E. De Marchi, A. Williamson, F. Di Virgilio, D. Heymann, E. Adinolfi, W.D. Fraser, D. Green, M.A. Lawson, A. Gartland, The P2RX7B splice variant modulates osteosarcoma cell behaviour and metastatic properties, *J. Bone Oncol.* 31 (2021) 100398.
- [22] M.I. Love, W. Huber, S. Anders, Moderated estimation of fold change and dispersion for RNA-seq data with DESeq2, *Genome Biol.* 15 (2014) 550.
- [23] D. Green, A. Singh, V.L. Tippett, L. Tattersall, K.M. Shah, C. Siachisumo, N.J. Ward, P. Thomas, S. Carter, L. Jeys, V. Sumathi, I. McNamara, D.J. Elliott, A. Gartland, T. Dalmay, W.D. Fraser, YBX1-interacting small RNAs and RUNX2 can be blocked in primary bone cancer using CADD522, *J. Bone Oncol.* 39 (2023) 100474.
- [24] D. Green, H. Eyre, A. Singh, J.T. Taylor, J. Chu, L. Jeys, V. Sumathi, A. Coonar, D. Rassl, M. Babur, D. Forster, S. Alzabin, F. Ponthan, A. McMahon, B. Bigger, T. Reekie, M. Kassiou, K. Williams, T. Dalmay, W.D. Fraser, K.G. Finegan, Targeting the MAPK7/MMP9 axis for metastasis in primary bone cancer, *Oncogene* 39 (33) (2020) 5553–5569.
- [25] V. Moravetski, J.R. Hill, U. Eichler, A.K. Cheetham, J. Sauer, 29Si NMR chemical shifts of silicate species: ab initio study of environment and structure effects, *J. Am. Chem. Soc.* 118 (51) (1996) 13015–13020.
- [26] C. Mercier, C. Follet-Houttemane, A. Pardini, B. Revel, Influence of P2O5 content on the structure of SiO2-Na2O-CaO-P2O5 bioglasses by 29Si and 31P MAS-NMR, *J. Non. Cryst. Solids*. 357 (24) (2011) 3901–3909.
- [27] J.H. Lopes, J.A. Magalhaes, R.F. Gouveia, C.A. Bertran, M. Motisuke, S.E.A. Camargo, E.S. Triches, Hierarchical structures of beta-TCP/45S5 bioglass hybrid scaffolds prepared by gelcasting, *J. Mech. Behav. Biomed. Mater.* 62 (2016) 10–23.
- [28] C.C. Lin, L.C. Huang, P. Shen, Na2CaSi2O6–P2O5 based bioactive glasses. Part 1: elasticity and structure, *J. Non. Cryst. Solids*. 351 (40–42) (2005) 3195–3203.
- [29] F. Miyaji, S. Sakka, Structure of PbO-Bi2O3-Ga2O3 glasses, *J. Non. Cryst. Solids*. 134 (1–2) (1991) 77–85.
- [30] Z. Xu, X. Zhao, X. Chen, Z. Chen, Z. Xia, Antimicrobial effect of gallium nitrate against bacteria encountered in burn wound infections, *RSC. Adv.* 7 (2017) 52266–52273.
- [31] F. Kurtuldu, N. Mutlu, A.R. Boccaccini, D. Galusek, Gallium containing bioactive materials: a review of anticancer, antibacterial, and osteogenic properties, *Bioact. Mater.* 17 (2022) 125–146.
- [32] S. Crunkhorn, Gallium fights infection in phase I trial, *Nat. Rev. Drug Discov.* 17 (2018) 786.
- [33] A. Elfadadny, R.F. Ragab, M. AlHarbi, F. Badshah, E. Ibáñez-Arancibia, A. Farag, A.O. Hendawy, P.R. De los Ríos-Escalante, M. Aboubakr, S.A. Zakai, W.M. Nageeb, Antimicrobial resistance of *Pseudomonas aeruginosa*: navigating clinical impacts, current resistance trends, and innovations in breaking therapies, *Front. Microbiol.* 15 (2024) 2024.
- [34] P. Hernández-Jiménez, F. López-Medrano, M. Fernández-Ruiz, J.T. Silva, L. Corbella, R. San-Juan, M. Lizasoain, J. Díaz-Regañón, E. Viedma, J.M. Aguado, Risk factors and outcomes for multidrug resistant *Pseudomonas aeruginosa* infection in immunocompromised patients, *Antibiotics* 11 (11) (2022) 1459.
- [35] L.R. Bernstein, Mechanisms of therapeutic activity for Gallium, *Pharmacol. Rev.* 50 (4) (1998) 665–682.
- [36] C.R. Chitambar, Gallium and its competing roles with iron in biological systems, *Biochim. Biophys. Acta (BBA) - Mol. Cell Res.* 1863 (8) (2016) 2044–2053.
- [37] S.B. Owusu, A. Zaher, S. Ahenkorah, D.N. Pandya, T.J. Wadas, M.S. Petronek, Gallium uncouples iron metabolism to enhance glioblastoma radiosensitivity, *Int. J. Mol. Sci.* 25 (18) (2024) 10047.
- [38] A. Zoccarato, I. Smyrniak, C.M. Reumiller, A.D. Hafstad, M. Chong, D.A. Richards, C.X.C. Santos, A. Visnagri, S. Verma, D.I. Bromage, M. Zhang, X. Zhang, G. Sawyer, R. Thompson, A.M. Shah, NRF2 activation in the heart induces glucose metabolic reprogramming and reduces cardiac dysfunction via upregulation of the pentose phosphate pathway, *Cardiovasc. Res.* 121 (2) (2025) 339–352.
- [39] B.M. Hybertson, B. Gao, S.K. Bose, J.M. McCord, Oxidative stress in health and disease: the therapeutic potential of Nrf2 activation, *Mol. Asp. Med.* 32 (4) (2011) 234–246.
- [40] A.M. Sherwood, B.A. Yasseen, J.M. DeBlasi, S. Caldwell, G.M. DeNicola, Distinct roles for the thioredoxin and glutathione antioxidant systems in Nrf2-mediated lung tumor initiation and progression, *Redox. Biol.* 83 (2025) 103653.
- [41] D. Romani, F. Marchetti, C. Di Nicola, M. Cuccioloni, C. Gong, A.M. Eleuteri, A. Galindo, F. Fadaei-Tirani, M. Nabissi, R. Pettinari, Multitarget-directed gallium(III) tris(acetyl-pyrazolonate) complexes induce ferroptosis in cancer cells via dysregulation of cell redox homeostasis and inhibition of the mevalonate pathway, *J. Med. Chem.* 66 (5) (2023) 3212–3225.
- [42] Y. Tanaka, A. Nakamura, M.S. Morioka, S. Inoue, M. Tamamori-Adachi, K. Yamada, K. Taketani, J. Kawachi, M. Tanaka-Okamoto, J. Miyoshi, H. Tanaka, S. Kitajima, Systems analysis of ATF3 in stress response and cancer reveals opposing effects on pro-apoptotic genes in p53 pathway, *PLoS. One* 6 (10) (2011) e26848.
- [43] X. Bao, N. Zhang, C. Wang, S. Liu, A. Fan, F. Zheng, C. Yang, KRAS regulates IL-17 signal activity by affect the metastasis of osteosarcoma via an IL-17A-dependent manner, *JBM. Plus.* 9 (7) (2025).
- [44] P. Uniyal, V.K. Kashyap, T. Behl, D. Parashar, R. Rawat, KRAS mutations in cancer: understanding signaling pathways to immune regulation and the potential of immunotherapy, *Cancers* 17 (5) (2025) 785.
- [45] J. Gonzalez-Molina, S. Gramolelli, Z. Liao, J.W. Carlson, P.M. Ojala, K. Lehti, MMP14 in Sarcoma: a regulator of tumor microenvironment communication in connective tissues, *Cells* 8 (9) (2019) 991.
- [46] D.M. Xu, L.X. Chen, T. Xue, X.Y. Zhuang, L.C. Wei, H. Han, M. Mo, Decoding the impact of MMP1 + malignant subsets on tumor-immune interactions: insights from single-cell and spatial transcriptomics, *Cell Death. Discov.* 11 (2025) 244.
- [47] L. Ding, T. Liu, Y. Qu, Z. Kang, L. Guo, H. Zhang, J. Jiang, F. Qu, W. Ge, S. Zhang, Lncrna MELTF-AS1 facilitates osteosarcoma metastasis by modulating MMP14 expression, *Mol. Ther. Nucl. Acids*. 26 (2021) 787–797.
- [48] O. Doppelt-Flikshtain, T. Asbi, A. Younis, O. Ginesin, Z. Cohen, T. Tamari, T. Berg, C. Yanovich, D. Aran, Y. Zohar, Y.G. Assaraf, H. Zigdon-Giladi, Inhibition of osteosarcoma metastasis in vivo by targeted downregulation of MMP1 and MMP9, *Matrix. Biol.* 134 (2024) 48–58.
- [49] M. Mahdizadehi, M. Saghaeian Jazi, S.M. Mir, S.M. Jafari, Role of fibrilins in human cancer: a narrative review, *Health Sci. Rep.* 6 (2023) e1434.
- [50] S. Chen, Y. Li, Y. Zhu, J. Fei, L. Song, G. Sun, L. Guo, X. Li, SERPINE1 Overexpression promotes malignant progression and poor prognosis of gastric cancer, *J. Oncol.* 2022 (2022) 2647825.
- [51] S. Polo-Generelo, C. Rodríguez-Mateo, B. Torres, J. Pintor-Tortolero, J.A. Guerrero-Martínez, J. König, J. Vázquez, E. Bonzón-Kulichenko, J. Padillo-Ruiz, F. de la Portilla, J.C. Reyes, J.A. Pintor-Toro, Serpine1 mRNA confers mesenchymal characteristics to the cell and promotes CD8 + T cells exclusion from colon adenocarcinomas, *Cell Death. Discov.* 10 (2024) 116.
- [52] Q. Liu, A. Li, Y. Tian, J.D. Wu, Y. Liu, T. Li, Y. Chen, X. Han, K. Wu, The CXCL8-CXCR1/2 pathways in cancer, *Cytokine Growth Factor Rev.* 31 (2016) 61–71.
- [53] X. Xiong, X. Liao, S. Qiu, H. Xu, S. Zhang, S. Wang, J. Ai, L. Yang, CXCL8 in tumor biology and its implications for clinical translation, *Front. Mol. Biosci.* 9 (2022) 723846.
- [54] L. Meng, Y. Zhao, W. Bu, X. Li, X. Liu, D. Zhou, Y. Chen, S. Zheng, Q. Lin, Q. Liu, H. Sun, Bone mesenchymal stem cells are recruited via CXCL8-CXCR2 and promote EMT through TGF- β signal pathways in oral squamous carcinoma, *Cell Prolif.* 53 (2020) e12859.
- [55] S. Sheng, The feasibility of uPA/uPAR-targeting strategies in cancer treatment, *Cancer Biol. Ther.* 7 (5) (2008) 660–662.
- [56] T. Lv, Y. Zhao, X. Jiang, H. Yuan, H. Wang, X. Cui, J. Xu, J. Zhao, J. Wang, uPAR: an essential factor for tumor development, *J. Cancer* 12 (23) (2021) 7026–7040.
- [57] X.W. Yu, T.Y. Wu, X. Yi, W.P. Ren, Z.B. Zhou, Y.Q. Sun, C.Q. Zhang, Prognostic significance of VEGF expression in osteosarcoma: a meta-analysis, *Tumor Biol.* 35 (2014) 155–160.
- [58] C.C. Chao, W.F. Lee, W.H. Yang, C.Y. Lin, C.K. Han, Y.L. Huang, Y.C. Fong, M.H. Wu, I.T. Lee, Y.H. Tsai, C.H. Tang, J.F. Liu, IGFBP-3 stimulates human osteosarcoma cell migration by upregulating VCAM-1 expression, *Life Sci.* 265 (2021) 118758.
- [59] G.M. Guimarães, F. Tesser-Gamba, A.S. Petrilli, M.T.S. Alves, R.J. Garcia-Filho, R. Oliveira, S.R.C. Toledo, IGFBP5 in osteosarcoma tumorigenesis: gene expression profile among metastatic and non-metastatic patients, *Gene* 934 (2025) 149026.
- [60] A. Hosseini, A. Mirzaei, V. Salimi, K. Jamshidi, P. Babaheidarian, S. Fallah, Z. Rampishah, N. Khademi, Z. Abdolvahabi, M. Bahrabadi, M. Ibrahim, F. Hosami, M. Tavakoli-Yaraki, The local and circulating SOX9 as a potential biomarker for the diagnosis of primary bone cancer, *J. Bone Oncol.* 23 (2020) 100300.
- [61] C.R. Chitambar, Gallium-containing anticancer compounds, *Future Med. Chem.* 4 (10) (2012) 1257–1272.
- [62] R.P. Warrell Jr., C.J. Coonley, D.J. Straus, C.W. Young, Treatment of patients with advanced malignant lymphoma using gallium nitrate administered as a seven-day continuous infusion, *Cancer* 51 (11) (1983) 1982–1987.
- [63] C.R. Chitambar, The therapeutic potential of iron-targeting gallium compounds in human disease: from basic research to clinical application, *Pharmacol. Res.* 115 (2017) 56–64.
- [64] M. Kurtjak, M. Vukomanović, L. Kramer, D. Suvorov, Biocompatible nano-gallium/hydroxyapatite nanocomposite with antimicrobial activity, *J. Mater. Sci.* 27 (2016) 170.
- [65] C.H. Goss, Y. Kaneko, L. Khuu, G.D. Anderson, S. Ravishanker, M.L. Aitken, N. Lechtzin, G. Zhou, D.M. Czyz, K. McLean, O. Olakanmi, H.A. Shuman, M. Teresi, E. Wilhelm, E. Caldwell, S.J. Salpante, D.B. Hornick, R.J. Siehnel, L. Becker, B.E. Britigan, P.K. Singh, Gallium disrupts bacterial iron metabolism and has therapeutic effects in mice and humans with lung infections, *Sci. Transl. Med.* 10 (460) (2018) eaat7520.